Nuclear Instruments and Methods in Physics Research A 1059 (2024) 169002

Contents lists available at ScienceDirect

Nuclear Inst. and Methods in Physics Research, A

journal homepage: www.elsevier.com/locate/nima

Full Length Article

# Evaluation of rate capability of SiPM-based X-ray counting detector

V.V. Leonov [a], V.V. Porosev [a,b,*], G.A. Savinov [a]

[a] Budker Institute of Nuclear Physics, 11 Lavrentiev ave., Novosibirsk, 630090, Russia
[b] Novosibirsk State University, 1, Pirogova str., Novosibirsk, 630090, Russia

ARTICLE INFO

*Keywords:*
X-ray detector
Photon counting detectors
Silicon photomultipliers

ABSTRACT

Scintillation radiation detectors based on silicon photomultipliers (SiPMs) are widely used nowadays both in various medical apparatus and physics experiments, e.g., in PET. At the same time, this technology has great potential in terms of creating X-ray photon counting detectors, which are in demand both in medicine and applied research. In this work, we investigate the influence of main SiPM parameters on the overall system performance, as well as different methods of data readout. It is shown that the use of SiPMs with shorter cell recovery time and larger number of microcells makes it possible to achieve a rate capability of 12 Mcps (mega counts per second) per channel. At the same time, the scintillator decay time is still among the limiting factors for such systems.

## 1. Introduction

Scintillation radiation detectors based on silicon photomultipliers (SiPMs) are widely used nowadays both in various medical and physics experiments [1], and such detectors are regarded as a potential alternative to CdTe and CZT detectors in photon-counting computer tomography (PCCT) [2–4]. We have recently developed a SiPM-based scintillation photon counting detector, which has proven the effectiveness of such systems for use in passenger screening systems [5]. The high throughput requirements of such systems limit the maximum inspection time to a few seconds, and detectors must be able to handle a high incident X-ray photon fluence rate at least of 4.5 Mcps per channel of ~2.5 mm$^2$. This value comes from the requirement of compliance with the safety standard, which limits the dose per screening to 0.25 $\mu Sv$ [6], and the need to obtain approximately a thousand image lines during a scanning time of 5 s. Enhancement of the detector count rate capability allows getting a detector response more close to linear, as well as provides higher image quality. In this work, we investigated the influence of a few detector parameters on the overall system performance, as well as different methods of data readout.

## 2. Influence of SiPM parameters on the detector counting rate

In general, the pulse shape of a scintillation detector is the convolution of the single-photoelectron response and an exponential function describing the luminescence profile of the scintillator. In the first approximation, the reaction of the silicon photomultiplier to an incident photon is the sum of two exponential dependences: fast discharge and slow recovery [7,8] and in a trivial case could be approximated as:

$$U(t) = \frac{A}{\tau_r - \tau_d}\left(e^{-\frac{t}{\tau_r}} - e^{-\frac{t}{\tau_d}}\right), \tag{1}$$

where $\tau_r$ and $\tau_d$ are constants describing the rise and decay time of the SiPM pulse when only one cell is fired. In principle, the rise time can be very fast (~100 ps). However, in many cases, the observed signal from a SiPM can have a slower rise time, e.g., due to the slew-rate and/or bandwidth limitations of the combined SiPM-readout circuit [9]. In this case, the averaged pulse shape at the output of the scintillation detector can be described by the following expression:

$$U(t) = AN_{sc} \cdot \frac{\tau_d(\tau_{sc}-\tau_r)\cdot e^{-\frac{t}{\tau_d}} - \tau_r(\tau_{sc}-\tau_d)\cdot e^{-\frac{t}{\tau_r}} + \tau_{sc}(\tau_r-\tau_d)\cdot e^{-\frac{t}{\tau_{sc}}}}{(\tau_{sc}-\tau_r)(\tau_{sc}-\tau_d)(\tau_r-\tau_d)} \cdot \theta(t), \tag{2}$$

where $N_{sc}$ is the total number of scintillation photons, $\tau_{sc}$ is the decay constant of the scintillator, and $\theta(t)$ is the unit step function. Fig. 1 illustrates the influence of the cell recovery time $\tau_d$ on the detector pulse duration for a scintillator with decay time $\tau_{sc}$ of 40 ns and SiPM pulse rise time of 2 ns. It is well seen that a longer cell recovery time considerably increases the pulse duration and leads to a significantly higher probability of pile-up. In addition, for the given values of parameters, the time to reach the maximum signal is well approximated by the cell recovery time.

* Corresponding author at: Budker Institute of Nuclear Physics, 11 Lavrentiev ave., Novosibirsk, 630090, Russia.
*E-mail address:* porosev@inp.nsk.su (V.V. Porosev).

https://doi.org/10.1016/j.nima.2023.169002
Received 25 October 2023; Received in revised form 27 November 2023; Accepted 5 December 2023
Available online 7 December 2023

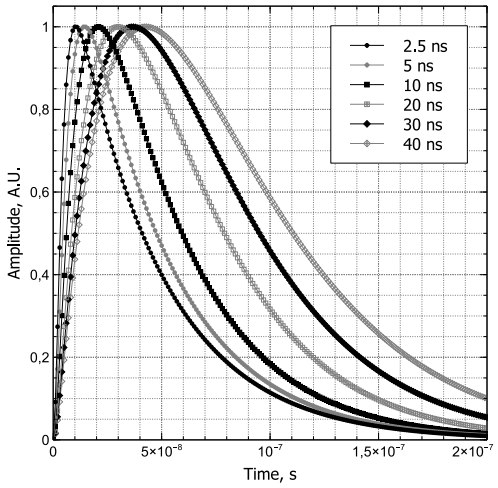


**Fig. 1.** Averaged detector pulse shape with 40 ns scintillator luminescence time at different SiPM cell recovery times.

**Table 1**
Main parameters of SiPMs used in experiments.

| | PM1125 | S14160-1315PS |
|---|---|---|
| Active area, mm | 1.2 × 1.2 | 1.3 × 1.3 |
| Pixel pitch, μm | 25 × 25 | 15 × 15 |
| Number of micro-cells, | 2304 | 7284 |
| Cell recovery time, ns | 40 | 15 |
| Breakdown voltage, V | ~28 | ~38 |
| Gain | $1.0 \times 10^6$ | $3.6 \times 10^5$ |

**Table 2**
Estimated parameters of detector response.

| | PM1125 | | S14160-1315PS | |
|---|---|---|---|---|
| | $\tau_r$, ns | $\tau_d$, ns | $\tau_r$, ns | $\tau_d$, ns |
| LED | $2.8 \pm 0.2$ | $36.6 \pm 0.7$ | $2.9 \pm 0.2$ | $15.5 \pm 0.5$ |
| Am-241 | $30.5 \pm 1.4$ | $57.4 \pm 2.2$ | $16.5 \pm 0.7$ | $39.7 \pm 1.2$ |

To validate this issue, we performed a comparative study of S14160-1315PS (HAMAMATSU) and PM1125 (KETEK) silicon photomultipliers. Table 1 presents the main parameters of the SiPMs used.

The SiPMs were mounted in a light-tight box and irradiated with SP5601 LED Driver (CAEN). The signals from the sense resistor of 50 Ohm were amplified with a home-made amplifier based on OPA847 (Texas Instruments) with gain of ~50. The data were sampled and read out with application of a Tektronix DPO3032 oscilloscope and averaged off-line. In another test, we mounted a teflon wrapped LFS-3 scintillator crystal (light yield 29 ph/keV, decay time 40 ns) with dimensions of 1.5 × 1.5 × 3.5 mm on the SiPM entrance window with MELMOUNT 1.582 grease and irradiated it with Am-241 isotope. Fig. 2 and Table 2 demonstrate averaged detector profiles and estimated decay and rise time constants.

As expected, the SiPM cell recovery time considerably influences the detector pulse width and would limit the maximal reachable counting rate.

## 3. SiPM-based scintillation detector

To evaluate the SiPM response influence on the count-rate capability of a detector, we compared performance of two 32-channel readout modules based on different SiPM models using the LFS-3 scintillator (Zecotek). The scintillator crystals have dimensions of 1.5 × 1.5 × 3.5 mm, and the pitch of the detector channels is 1.6 mm. All scintillator crystals are wrapped with Enhanced Specular Reflector Film (3M™) and jointed to individual SiPMs with MELMOUNT 1.582 optical grease. The cathodes of the SiPMs are connected to a common high-voltage power supply, whereas the anodes are loaded by a resistor (30 Ω typically), followed by a decoupling capacitor. The detector electronics are based on a 32-channel Omega EASIROC (old version)/CITIROC front-end ASICs [10,11]. Each ASIC channel incorporates an integrated front-end DAC for SiPM operation voltage adjustment in the range from 0 to 4.5 V (3.5 V typically), adjustable gain preamplifier, and a 15-ns peaking-time fast shaper, followed by a discriminator. The common threshold for all the discriminators is set by an integrated 10-bit DAC. The trigger outputs come to an FPGA, which counts the number of the events in each channel, when the signal level of the outputs of the fast shapers exceeds the threshold. The detector was installed on a scanning radiography system equipped with an X-ray tube RTM101 (IAE, Italy) with focal spot size of 0.6 mm and focus-to-detector distance of 1350 mm. A collimator with a 1 mm slit, located at a distance of 650 mm from the focus of the tube, forms a narrow fan-shaped radiation beam. The general view of the detector boards and a typical pulse at the output of a fast bipolar shaper are presented in Fig. 3. It can be seen that the width of the pulse depends on its amplitude. In addition, the signal at the output of the ASIC bipolar fast shaper exhibits a nonlinear response with some pulse shape distortion at large pulse amplitudes [12,13]. All these factors will form rather complex behavior of the detector.

## 4. Evaluation of dead time

The dead time dramatically influences the statistics of recorded events [14] and distorts the time-interval distribution. For a perfect detector, the time-interval distribution is just an exponential distribution, which describes the time between events in a Poisson process. For a non-paralyzable counter with dead-time $\tau$, the time-interval distribution is represented by a shifted exponential:

$$F(t) = \Theta(t-\tau) N e^{-N(t-\tau)}, \tag{3}$$

where $N$ is the input flux, whereas for the extended (paralyzable) dead time it takes a more complex form [15,16]:

$$F(t) = N \sum_{j=1}^{\infty} \Theta(t-j\tau) \frac{(-N(t-j\tau))^{j-1}}{(j-1)!} e^{-jN\tau}. \tag{4}$$

Therefore, evaluation of time-interval distribution is an effective method of system assessment to understand its behavior. Real systems consist of a series-connected detector and electronic modules, which can have their own dead times, which leads to an even more complex detector behavior. To get the time-interval distributions of our detector, we recorded trigger outputs of the front-end ASIC with a Tektronix DPO3032 oscilloscope during irradiation and performed off-line analysis.

## 5. Results and discussion

Fig. 4 demonstrates the time-interval distributions for two types of detector boards at the same irradiation conditions, and Fig. 5 shows an example of the 2D pulse width versus the time-interval distribution for a low intensity condition (80 kVp, 5 mA).

The specific shape of the distributions (with a flat part in the area of the maximum values) demonstrates the presence of paralyzing dead-time in the readout channels. Besides, the KETEK SiPM-based detector demonstrates abnormal behavior at input rates above 15 Mcps (the X-ray tube currents exceeding 20 mA). This complicate detector behavior can be explained by a few reasons. Firstly, at a high X-ray intensity, a limited number of microcells with rather slow recovery do not have time for recharge between successive events, and thus the amplitude of some of events is below the detection threshold. Another important factor which affects the detector behavior is the limited sink capability of the input DACs of the ASICs. At high X-ray intensity,

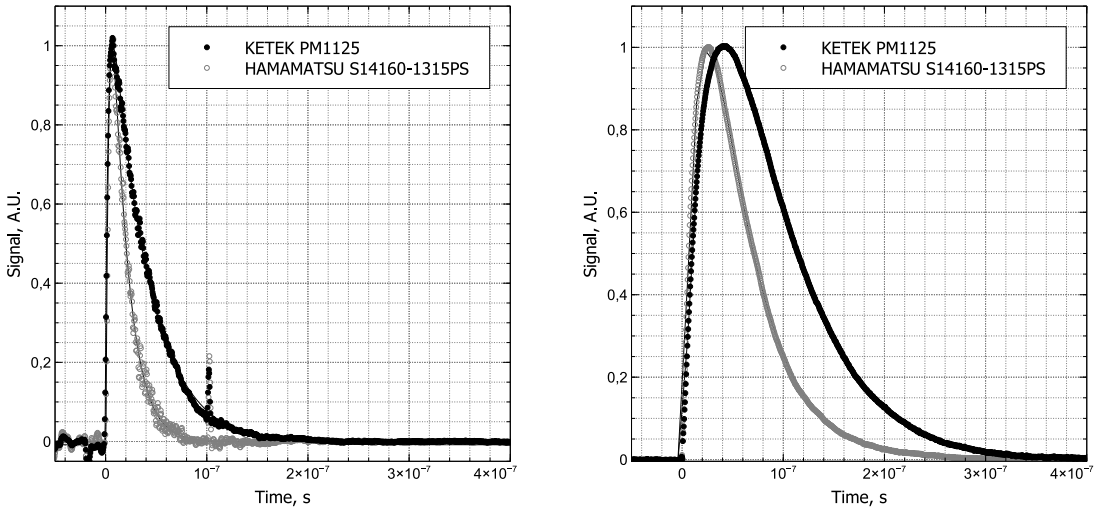


**Fig. 2.** Averaged SiPM response for KETEK PM1125 and HAMAMATSU S14160-1315PS under irradiation with LED (left) and with mounted LFS-3 scintillator and irradiation with Am-241 (right).

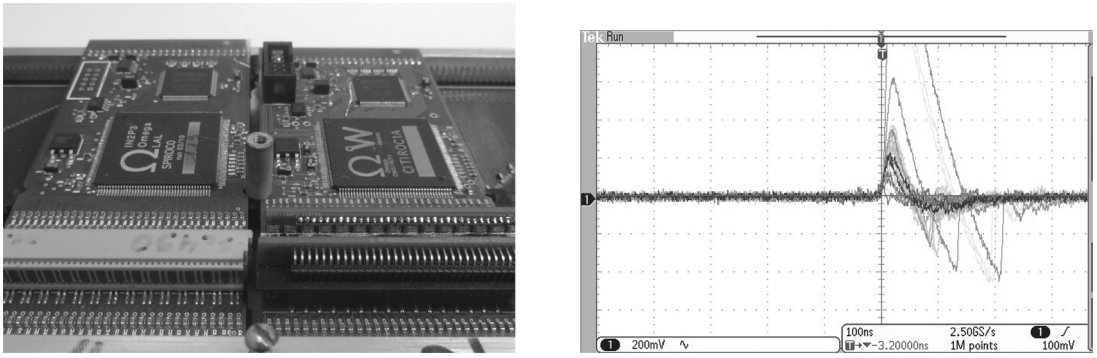


**Fig. 3.** General design of detector boards with KETEK and HAMAMATSU micropixel photon counters (left) and pulses at outputs of ASIC fast shaper (right).

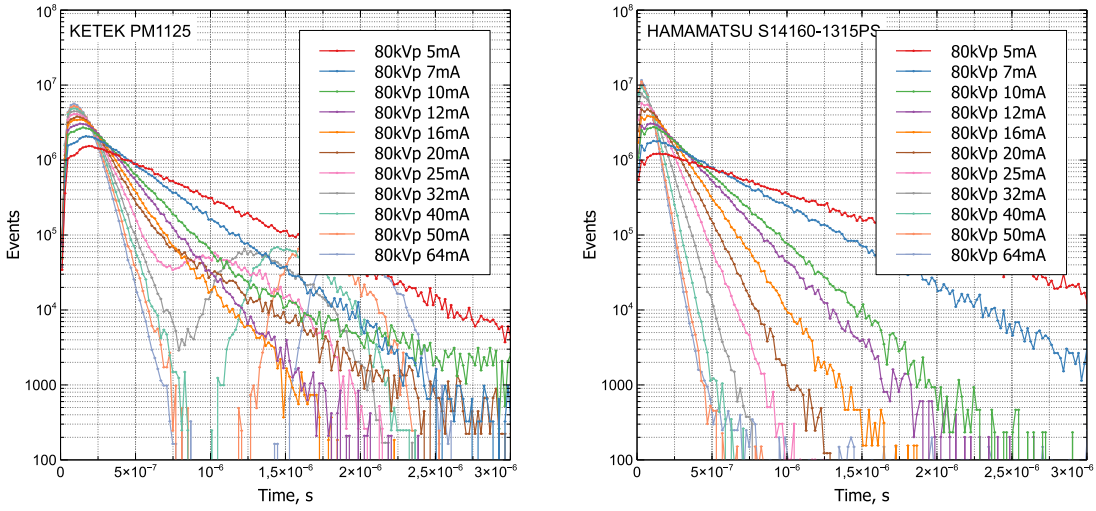


**Fig. 4.** Time-interval distribution of KETEK SiPM- (left) and HAMAMATSU MPPC- (right) based detectors at different irradiation conditions.

they cannot maintain a constant potential, which leads to a decrease in the gain of the SiPMs and, as a consequence, loss of some events. For HAMAMATSU MPPCs, the small cell recovery time leads to higher probability of generation of a few short trigger pulses per one detected photon. Nevertheless, such SiPMs with smaller cell size and gain have a benefit of the generation of lower average current and as a result, more stable MPPC operation at high input intensities. In any case, a broad spectrum of X-ray photons leads to the formation of large spread in the width of recorded pulses. Based on this data, we formed a minimum pulse width of ~30 ns into the FPGA logic using an external clock upstream of all counters. Since pulses with a KETEK SiPM have a longer duration and, accordingly, a greater probability of pile-up,

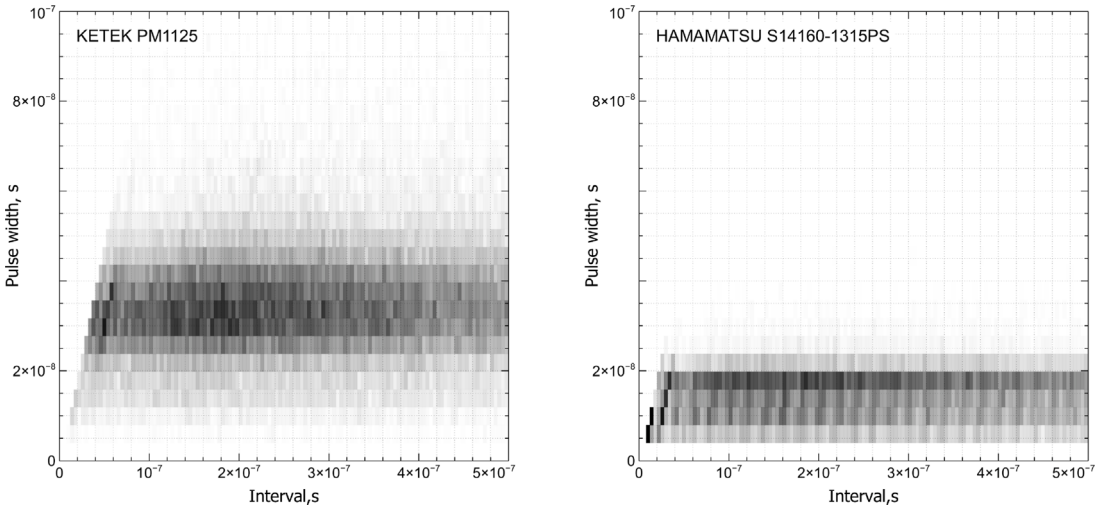


**Fig. 5.** Pulse width versus time-interval of detectors based on KETEK SiPM (left) and HAMAMATSU MPPC (right).

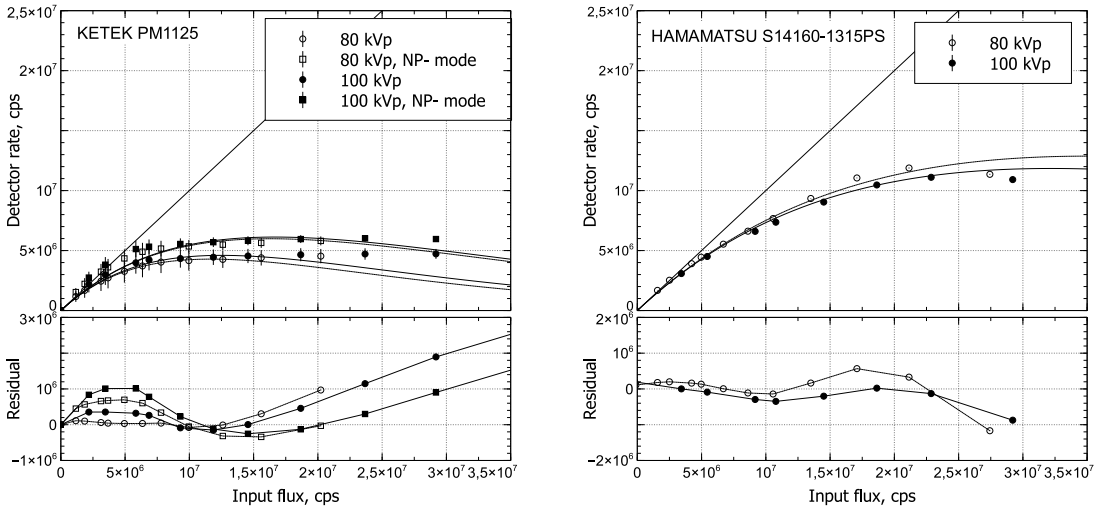


**Fig. 6.** Detection rate with detectors based on KETEK SiPMs in standard and re-trigger (NP) mode (left) and on HAMAMATSU MPPC (right) together with residual errors of fits.

we additionally tested the re-trigger mechanism [17]. In this case, if the pulse amplitude was above the threshold for a time exceeding the standard pulse duration ~50 ns, the trigger signal was re-generated, and in such way we could realize a non-paralyzable counting mode. Fig. 6 demonstrates the detector rate capability as a function of the input flux for the mentioned readout techniques.

The straight line demonstrates the "ideal" detector response, and the non-linear curves present results of fits with the hybrid dead-time model [18]. In this model, the observed count rate is defined as

$$N_{obs} = \frac{N \cdot e^{-N f \tau}}{1 + N \cdot (1 - f) \cdot \tau}, \tag{5}$$

where $N, \tau_d$, and $f$ are the true count rate, the dead time, and the paralysis factor, correspondingly. In the case of an ideally paralyzing detector $f$ would be 1, and for an ideally nonparalyzing detector it would be 0. We also added for comparison data at 100 kVp to see possible deviations for a slightly different X-ray spectrum. Table 3 summarizes the estimated parameters.

In all cases, the detector demonstrates the pure paralyzed behavior. Anyway, for a KETEK SiPM, the detector demonstrates quite a bad match of experimental data with the simplified model. The re-trigger readout mode with a KETEK SiPM allowed extending the maximum count rate of the detector up to 6 MHz per channel. With a HAMAMATSU MPPC, the maximum count rate reaches 12 Mcps per channel, and the observed dead time is close to that implemented in the hardware.

**Table 3**
Estimated parameters of fits at different irradiation conditions.

| | 80 kVp | | 100 kVp | |
|---|---|---|---|---|
| | f | $\tau$, ns | f | $\tau$, ns |
| PM1125, P-mode | 1.0 | $83 \pm 7$ | 1.0 | $80 \pm 7$ |
| PM1125, NP-mode | 1.0 | $61 \pm 4$ | 1.0 | $60 \pm 3$ |
| S14160-1315PS | $1.00 \pm 0.03$ | $30 \pm 1$ | $1.00 \pm 0.03$ | $31 \pm 1$ |

## 6. Conclusion

In this research we tried to find a way to improve the count rate capabilities of the SiPM-based scintillation detector. As expected, along with the scintillator decay time, the micro-cell recovery time has significant influence on the detector performance. Application of a SiPM with a smaller microcell size and faster recovery enables significant improvement of the detector rate capability, up to 12 Mcps per channel. Nevertheless, further progress in this field will be related

with the application of faster scintillators like LaBr3:Ce or hybrid organic–inorganic perovskite scintillators [19]. However, realization of re-trigger mode in readout electronics significantly improved the overall detector performance.

## CRediT authorship contribution statement

**V.V. Leonov:** Investigation. **V.V. Porosev:** Writing – review & editing, Writing – original draft, Investigation. **G.A. Savinov:** Investigation.

## Declaration of competing interest

The authors declare that they have no known competing financial interests or personal relationships that could have appeared to influence the work reported in this paper.

## Data availability

Data will be made available on request.

## Acknowledgments

This work was supported by the Ministry of Science and Higher Education of the Russian Federation. The author would like to thank I. Sokolova for the careful proofreading of this work.

## References

[1] S. Gundacker, A. Heering, The silicon photomultiplier: Fundamentals and applications of a modern solid-state photon detector, Phys. Med. Biol. 65 (17) (2020) 17TR01, http://dx.doi.org/10.1088/1361-6560/ab7b2d.

[2] Stefan van der Sar, Stefan Brunner, Dennis Schaart, X-ray photon-counting using silicon photomultiplier-based scintillation detectors at high x-ray tube currents, in: Proc. SPIE 12031, Medical Imaging 2022: Physics of Medical Imaging, http://dx.doi.org/10.1117/12.2611365.

[3] Stefan van der Sar, Stefan Brunner, Dennis Schaart, Silicon photomultiplier-based scintillation detectors for photon-counting CT: A feasibility study, Med. Phys. 48 (10) (2021) http://dx.doi.org/10.1002/mp.14886.

[4] M. Arimoto, et al., Development of 64-channel LSI with ultrafast analog and digital signal processing dedicated for photon-counting computed tomography with multi-pixel photon counter, Nucl. Instrum. Methods Phys. Res. A. 1047 (2023) http://dx.doi.org/10.1016/j.nima.2022.167721.

[5] E.A. Babichev, et al., Photon counting detector for the personal radiography inspection system SIBSCAN, Nucl. Instrum. Methods Phys. Res. A. 845 (2017) 499–502, http://dx.doi.org/10.1016/j.nima.2016.06.051.

[6] ANSI/HPS N43 17-2009, Radiation Safety for Personnel Security Screening Systems Using X-ray or Gamma Radiation.

[7] D. Marano, et al., Silicon photomultipliers electrical model extensive analytical analysis, IEEE Trans. Nucl. Sci. 61 (1) (2014) 23–34, http://dx.doi.org/10.1109/tns.2013.2283231.

[8] A.K. Jha, et al., Simulating silicon photomultiplier response to scintillation light, IEEE Trans. Nucl. Sci. 60 (1) (2013) 336–351, http://dx.doi.org/10.1109/TNS.2012.2234135.

[9] F. Acerbi, S. Gundacker, Understanding and simulating SiPMs, Nucl. Instrum. Methods Phys. Res. A. 926 (2019) 16–35, http://dx.doi.org/10.1016/j.nima.2018.11.118.

[10] S. Callier, et al., EASIROC, an easy and versatile readout device for SiPM, Phys. Procedia 37 (2012) 1569–1576, http://dx.doi.org/10.1016/j.phpro.2012.02.486.

[11] J. Fleury, et al., Petiroc and Citiroc: Front-end ASICs for SiPM read-out and ToF applications, JINST 9 (2014) C01049, http://dx.doi.org/10.1088/1748-0221/9/01/C01049.

[12] D. Impiombato, et al., Characterization of EASIROC as front-end for the readout of the SiPM at the focal plane of the Cherenkov telescope ASTRI, Nucl. Instrum. Methods Phys. Res. A. 729 (2013) 484–490, http://dx.doi.org/10.1016/j.nima.2013.07.029.

[13] E.A. Babichev, et al., SiPM based photon counting detector for scanning digital radiography, JINST 10 (2015) C03002, http://dx.doi.org/10.1088/1748-0221/10/03/C03002.

[14] D.F. Yu, J.A. Fessler, Mean and variance of single photon counting with deadtime, Phys. Med. Biol. 45 (7) (2000) 2043-2056, http://dx.doi.org/10.1088/0031-9155/45/7/324.

[15] S. Pomme, et al., Influence of pileup rejection on nuclear counting, viewed from the time-domain perspective, Nucl. Instrum. Methods Phys. Res. A. 426 (1999) 564–582, http://dx.doi.org/10.1016/S0168-9002(99)00016-9.

[16] S. Pomme, Time-interval distributions and counting statistics with a non-paralysable spectrometer, Nucl. Instrum. Methods Phys. Res. A. 437 (1999) 481–489, http://dx.doi.org/10.1016/s0168-9002(99)00791-3.

[17] T. Loeliger, et al., The new PILATUS3 ASIC with instant retrigger capability, in: 2012 IEEE Nuclear Science Symposium and Medical Imaging Conference Record (NSS/MIC) N6-2, 2012, pp. 610–615, http://dx.doi.org/10.1109/NSSMIC.2012.6551180.

[18] A. Patil, S. Usman, Measurement and application of paralysis factor for improved detector dead-time characterization, Nucl. Technol. 165 (2) (2009) 249–256, http://dx.doi.org/10.13182/NT09-A4090.

[19] J. Jasper van Blaaderen, et al., $(BZA)_2PbBr_4$: A potential scintillator for photon-counting computed tomography detectors, J. Lumin. 263 (2023) 120012, http://dx.doi.org/10.1016/j.jlumin.2023.120012.